Input-output analysis of the stochastic Navier-Stokes equations: Application to turbulent channel flow

Gilles Tissot [1,*] André V. G. Cavalieri [2] and Étienne Mémin[1]

[1]*INRIA Rennes Bretagne Atlantique, IRMAR–UMR CNRS 6625, 35042 Rennes, France*
[2]*Department of Aerospace Engineering, Instituto Tecnológico de Aeronáutica, Vila das Acácias, 12228-900, São José dos Campos, Brazil*

Stochastic linear modeling proposed in Tissot, Mémin, and Cavalieri [J. Fluid Mech. **912**, A51 (2021)] is based on classical conservation laws subject to a stochastic transport. Once linearized around the mean flow and expressed in the Fourier domain, the model has proven its efficiency to predict the structure of the streaks of streamwise velocity in turbulent channel flows. It has been in particular demonstrated that the stochastic transport by unresolved incoherent turbulence allows us to better reproduce the streaks through lift-up mechanism. In the present paper, we focus on the study of streamwise-elongated structures, energetic in the buffer and logarithmic layers. In the buffer layer, elongated streamwise vortices, named rolls, are seen to result from coherent wave-wave nonlinear interactions, which have been neglected in the stochastic linear framework. We propose a way to account for the effect of these interactions in the stochastic model by introducing a stochastic forcing, which replaces the missing nonlinear terms. In addition, we propose an iterative strategy in order to ensure that the stochastic noise is decorrelated from the solution, as prescribed by the modeling hypotheses. We explore the prediction abilities of this more complete model in the buffer and logarithmic layers of channel flows at $\mathrm{Re}_\tau = 180$, $\mathrm{Re}_\tau = 550$, and $\mathrm{Re}_\tau = 1000$. We show an improvement of predictions compared to resolvent analysis with eddy viscosity, especially in the logarithmic layer.

I. INTRODUCTION

Coherent structures of the near-wall turbulence is an extensively explored topic. In the buffer layer, very close to the wall, the flow organizes into streamwise vortices, or rolls, and elongated patterns of high or low streamwise velocity denoted as *streaks* [1–3]. These structures develop, break and are regenerated in a quasicyclical process [4]. A scenario explaining their behavior [5] considers the cycle where the streaks intensify by the lift-up mechanism [6,7] and destabilize by spanwise meandering, leading to nonlinear interactions which give finally birth to new streamwise vortices. This final step allows us to start a new cycle.

In the logarithmic layer, the flow organizes as well along streaks [8,9]. These structures are of larger size with a more disorganized motion due to the higher Reynolds number based on the wall distance (the wall distance in viscous units $y^+ = \frac{y u_\tau}{\nu}$ is a Reynolds number based on the friction velocity u_τ, the kinematic viscosity ν, and the wall distance in outer units y, the typical length scale of the largest structure [10]). Understanding their dynamical behavior is still an active research area. Smaller scales appear to be unnecessary to sustain these structures [11], suggesting the presence of a self-sustaining mechanism at large scale. Evidence indicates that this mechanism is similar to

---

*gilles.tissot@inria.fr

the one active in the buffer layer [12,13]. As noted in Cossu and Hwang [12], these large-scale coherent structures exist in the sense of (ensemble) averaging or filtering as associated to large eddy simulation. Even if they do not need the small scales to survive, they still interact with them. As a consequence, to predict their dynamical behavior, it is crucial to include the effect of small scales on these large scales through Reynolds stress models for instance or, as we propose here, by stochastic modeling. As a practical example in Bae *et al.* [14], resolvent analysis has been used to extract these large coherent structures in view of performing diagnostics of their action in removing their contributions in a numerical simulation. This procedure yields a drastic reduction of the turbulence intensity. The reduction is significant in the buffer layer and slightly less so in the logarithmic layer, highlighting the requirement of modeling improvements in this region. Besides, practical control strategies require an accurate prediction of these structures, and providing simplified models predicting coherent structures at a given scale with a high fidelity is still challenging.

By the knowledge of the time-averaged velocity field and possibly of some higher-order statistics, predicting coherent structures in a turbulent flow without resolving the whole multiscale space-time dependent solution has become an important research direction toward which many groups have devoted strong efforts. Considering a linearization of the Navier-Stokes operator around a suitably chosen flow—often taken as the time-averaged flow [15]—it is natural to search for wave solutions in the Fourier domain, which beyond a natural physical meaning gives access to efficient linear-algebra techniques. Since turbulence interacts with these wavy coherent structures, linearized solutions are often insufficient, and a closure is required.

Resolvent analysis [16–18] has become widely used to model coherent structures in turbulent flows since it considers the response of the linearized system to a forcing interpreted as the unknown nonlinear term [19]. By singular value decomposition (SVD) of the resolvent operator, optimal harmonic forcing modes and associated responses are found. Resolvent analysis is used for the modeling of dominant coherent structures in turbulent flows [14,19], data assimilation [20–25], as well as flow control [26]. The comparison between resolvent analysis and spectral proper orthogonal decomposition (SPOD) has been performed in turbulent channel flows at $Re_\tau = 180$ and 550 in Abreu *et al.* [27], where good agreement has been observed for elongated near-wall structures where the lift-up mechanism is active, associated with a dominance of the first SPOD mode. The main limitation of the method lies in the fact that coherent structures are well predicted if the nonlinear term can be approximated as a Gaussian white noise or if there is dominance of the first resolvent amplification gain (singular value) [28]. These conditions are often not verified.

In the context of a triple decomposition, where the velocity field is split into a time average, a coherent-structure component, and an incoherent turbulent field, an eddy viscosity can be introduced to the generalized Reynolds stresses induced by the incoherent part [29]. For streaky structures in turbulent channel flows Cess's eddy viscosity model [30] has proven its prediction efficiency to some extent [24,31–33], with a particular need in the logarithmic layer. In Morra *et al.* [34], it has been shown that the cross-spectral density (CSD) matrix of the nonlinear forcing in the DNS projects similarly onto resolvent forcing modes with eddy viscosity, thus explaining the improvement by adding an eddy viscosity. In Amaral *et al.* [24], resolvent-based estimations have been performed in turbulent channel flows at $Re_\tau = 180$, 550, and 1000. It has been shown that in the buffer layer, both resolvent with and without eddy viscosity lead to good estimations. However, in the logarithmic layer, adding eddy viscosity becomes necessary. Further improvement of estimation is possible if forcing statistics are used, without eddy viscosity, to build an optimal estimator. This allows estimating flow fluctuations from wall measurements at various wall-normal locations. Although using the CSD of the forcing terms is an interesting method to construct estimators, this is not a viable approach to predict dominant coherent structures in turbulent flows, as it requires extensive use of flow data.

Resolvent analysis with Cess's eddy viscosity will thus constitute our comparison model and will be referred to as ν_t-resolvent analysis, in contrast with ν-resolvent analysis when no eddy viscosity is considered. This works well for coherent structures, or waves, where strong production occurs. However, as argued by Symon *et al.* [35], since eddy viscosity is mainly diffusive (up to

eddy-diffusion gradients [36]), it breaks the energy conservation over the whole spectrum. Then, it is not well adapted for waves receiving energy from other scales by backscattering. A detailed study of the discrepancy of ν and ν_t-resolvent analysis for a turbulent channel flow in terms of low-rank property, projection onto SPOD modes and energy transfers can be found in Symon *et al.* [36]. Other attempts to improve the modeling have been proposed. The embedding of covariance informations of the forcing has been for instance proposed in Refs. [34,37]. However, this strategy was considered for diagnostic purposes only and has not been considered for predictions since a fine knowledge of the nonlinear term is in that case required. An estimator has been proposed by Gupta *et al.* [38] considering together eddy diffusion and a model of stochastic forcing. As an alternative in the temporal domain, Zare *et al.* [39,40] have devised a stochastic modeling based on control theory, which incorporates a coloured-in-time noise.

In Tissot *et al.* [41], a modeling strategy based on stochastic transport, so-called stochastic linear modes (SLM), has been proposed and will be considered in the present paper. It starts from a stochastic version of the Navier-Stokes equations, originally introduced by Mémin [42], which is based on the stochastic transport of conserved quantities. The formalism has been successfully employed to perform large eddy simulations [43], geophysical flow modeling [44–49], near-wall flow modeling [50], data assimilation [51–53], and reduced-order modeling [54,55]. An advantage of the approach is the formulation of closure by defining statistics of a stochastic unresolved time-decorrelated (with respect to the timescales of the contribution resolved by the model) velocity field. The associated random perturbation ensues then from a stochastic transport operator. This stochastic transport involves in addition a stochastic diffusion, and an effective drift velocity similar to the turbophoresis effect [56]. An exact energy balance is obtained between the stochastic diffusion and the energy backscattering induced by the stochastic transport [44]. Linearizing this model and expressing it in the Fourier domain leads to what we refer to as SLM.

In SLM, the nonlinear term, interpreted as the wave-wave interactions, has been neglected, relying on the stochastic transport of the solution by the incoherent turbulence to obtain a physically relevant model. In the present paper, we come back to this strong assumption. The generation of streamwise vortices likely involves nonlinear interactions between large-scale coherent structures. As will be detailed further, a close analysis of SLM for these elongated structures shows a poor prediction of the rolls, despite a good prediction of the streamwise velocity fluctuations. This is consistent with the fact that coherent wave-wave interactions are neglected in SLM. In order to recover the right roll properties, we propose in this paper to study the response of SLM to a "nonlinear" forcing similarly to what is done in resolvent analysis for modeling nonlinear effects through an input-output formalism. We name this enhanced solution *forced stochastic linear modes* (FSLM).

In addition to adding the aforementioned forcing, we propose some enhancements of the noise definition compared to Tissot *et al.* [41]. We propose an iterative procedure enforcing the noise to be incoherent with the solution. Moreover, the stochastic diffusion tensor is defined by root-mean-square velocity profiles in order to ensure an approximated consistency between stochastic diffusion and noise expressed in the Fourier domain. We propose as well a decorrelation time definition based on an inertial range scaling. Finally, SLM and FSLM numerical computation is improved by the reformulation of the equations as an SVD problem.

With this more complete model which incorporates the effect of time-decorrelated turbulence on the coherent structures, we will explore the prediction abilities of stochastic modeling in the buffer and logarithmic layer of three turbulent channel flows at friction Reynolds numbers $\mathrm{Re}_\tau = 180$, $\mathrm{Re}_\tau = 550$, and $\mathrm{Re}_\tau = 1000$. In particular, we will explore the ability of FSLM to predict coherent structures in the logarithmic layer.

In Sec. II, notations used along the paper are introduced. In Sec. III, we present the stochastic model. In Sec. IV we explore the ability of these models to predict buffer and logarithmic layer structures in turbulent channel flows. Some modeling recommendations are given in Sec. V. Conclusions are provided in Sec. VI. Presentation of the resolvent analysis, numerical details, and

complementary results are given in Supplemental Material [57] in order to have a more complete view by varying Reynolds number and sweeping the wave-number space.

II. NOTATIONS AND PRELIMINARIES

We consider three turbulent channel flows at the friction Reynolds numbers $Re_\tau = 180$, $Re_\tau = 550$, and $Re_\tau = 1000$ with the Cartesian coordinates $\boldsymbol{x} = (x, y, z)$ of the streamwise, wall-normal, and spanwise directions of the domain Ω, respectively. The domain sizes (L_x, L_y, L_z) in outer units are respectively $(4\pi, 2, 2\pi)$, $(2\pi, 2, \pi)$, and $(2\pi, 2, \pi)$. Details and validations of the flow simulations can be found in Ref. [24], and additional details at $Re_\tau = 550$ are present in Ref. [34]. The time-dependent (t) state variable $\boldsymbol{q}(x, y, z, t) = (\boldsymbol{u}, p)^T$ is composed of the velocity vector $\boldsymbol{u} = (u, v, w)^T$ and the pressure p. The velocity field is decomposed in its time-average and fluctuation $\boldsymbol{u} = \bar{\boldsymbol{u}} + \boldsymbol{u}'$ with $\bar{\boldsymbol{u}} = (U(y), 0, 0)^T$. By periodicity in the streamwise (x) and spanwise (z) directions, the space-time Fourier coefficient of the state variable with the sign convention $e^{i(\alpha x + \beta z - \omega t)}$ is noted $\hat{\boldsymbol{q}}_{\alpha,\beta,\omega}(y)$. Variables α, β, and ω refer respectively to streamwise wave number, spanwise wave number, and angular frequency. In the wall-normal direction, we define a diagonal matrix $\mathbf{W}$ of quadrature coefficients. Finally, we note $\cdot^H$ the transpose-conjugate operation.

III. STOCHASTIC LINEAR MODEL AND NONLINEAR FORCING

A. Stochastic linear modes

In Tissot *et al.* [41], a modeling strategy for coherent structures in turbulent flows has been proposed. The formalism relies on the stochastic transport of conserved quantities by a time-differentiable velocity component perturbed by the variation of a Brownian motion. Under these assumptions a stochastic version of the Navier-Stokes equations under location uncertainty [42] can be written. In this section, we recall how the stochastic model can be expressed in the frequency-wave-number domain to predict coherent structures. More details can be found in Tissot *et al.* [41].

The displacement $\boldsymbol{X}(\boldsymbol{x}, t)$ of a particle is written in a differential form,

$$dX(\boldsymbol{x}, t) = \boldsymbol{u}(\boldsymbol{x}, t)dt + (\boldsymbol{\sigma} d\boldsymbol{B}_t)(\boldsymbol{x}), \tag{1}$$

where $\boldsymbol{u}$ is a time-differentiable velocity component and $d\boldsymbol{B}_t$ is the increment of a Brownian motion. It can be remarked that Eq. (1) has to be understood as a time integral over an infinitesimal time increment dt. The operator $\boldsymbol{\sigma}$ is an integral operator which hides a spatial convolution in the domain Ω with a user-defined kernel $\check{\boldsymbol{\sigma}}$,

$$(\boldsymbol{\sigma} d\boldsymbol{B}_t)^i(\boldsymbol{x}) = \int_\Omega \check{\boldsymbol{\sigma}}^{ij}(\boldsymbol{x}, \boldsymbol{x}', t) d\boldsymbol{B}_t^j(\boldsymbol{x}') \, d\boldsymbol{x}', \tag{2}$$

where the indices i and j refer to component indices. The vector $\boldsymbol{x}'$ is composed of the integration space coordinates.

Defined as such, $\boldsymbol{\sigma} d\boldsymbol{B}_t$ is the displacement field induced by a velocity component that is smooth in space but decorrelated in time. This term aims at representing a time decorrelated (with respect to the timescale of the considered physical processes) turbulent velocity component. In the general framework, $\boldsymbol{\sigma}$ can be smoothly time dependent, but for the application of the present paper in statistically stationary turbulent flows, we will assume it constant in time.

Associated with $\boldsymbol{\sigma}$, we define the variance tensor $\mathbf{a}$ such that

$$\mathbf{a}_{ij}(\boldsymbol{x})dt = \mathbb{E}((\boldsymbol{\sigma} d\boldsymbol{B}_t)^i(\boldsymbol{x})(\boldsymbol{\sigma} d\boldsymbol{B}_t)^j(\boldsymbol{x})), \tag{3}$$

with $(\boldsymbol{\sigma} d\boldsymbol{B}_t)^i(\boldsymbol{x})$ the ith component of $\boldsymbol{\sigma} d\boldsymbol{B}_t$ at position $\boldsymbol{x}$ and $\mathbb{E}$ the expectation operator.

Using the Itō-Wentzell formula, conservation of mass and momentum subject to a stochastic transport leads to a stochastic version of the incompressible Navier-Stokes equations [42,44],

referred to as *under location uncertainty*:

$$d_t\boldsymbol{u} + (\boldsymbol{u}_d \cdot \nabla)\boldsymbol{u}\, dt + (\boldsymbol{\sigma} d\boldsymbol{B}_t \cdot \nabla)\boldsymbol{u} = -\nabla(p_t\, dt + dp_t) + \frac{1}{\text{Re}}\nabla \cdot (\nabla\boldsymbol{u})\, dt$$

$$+ \nabla \cdot \left(\frac{1}{2}\mathbf{a}\nabla\boldsymbol{u}\right) dt + \frac{1}{\text{Re}}\nabla \cdot (\nabla\boldsymbol{\sigma} d\boldsymbol{B}_t)$$

$$\nabla \cdot \boldsymbol{u}_d = 0; \quad \nabla \cdot \boldsymbol{\sigma} = 0,$$

$$\boldsymbol{u}_d = \boldsymbol{u} - \frac{1}{2}\nabla \cdot \mathbf{a}. \tag{4}$$

In system (4), Re is the Reynolds number. Compared to the deterministic case, the transport of $\boldsymbol{u}$ by $\boldsymbol{\sigma} d\boldsymbol{B}_t$ is introduced. This term brings energy (backscatter) to the system, which is exactly compensated by the stochastic diffusion $\nabla \cdot (\frac{1}{2}\mathbf{a}\nabla\boldsymbol{u})\, dt$ [44]. The variable $\boldsymbol{u}_d$ is called *drift velocity*. It takes into account that, on average, particles tend to be transported from highly turbulent regions toward low-turbulence regions (see Ref. [54] and references therein). Mass conservation leads to a divergence-free condition on $\boldsymbol{u}_d$ and on $\boldsymbol{\sigma}$. Finally, a random pressure term dp_t corresponding to the small-scale velocity component is involved. This force balances the martingale part (proportional to $d\boldsymbol{B}_t$) of the system.

In Tissot *et al.* [41], system (4) is linearized around a mean velocity profile $U(y)$ and written in the Fourier domain (see details of the derivation in the latter reference), leading to

$$-i\omega\hat{u}_{\alpha,\beta,\omega} + i\alpha U_d\hat{u}_{\alpha,\beta,\omega} + \hat{v}_{\alpha,\beta,\omega}\frac{\partial U}{\partial y} + i\alpha\hat{p}_{\alpha,\beta,\omega} + \widetilde{D}(\hat{u}_{\alpha,\beta,\omega}) = -(\dot{\boldsymbol{\xi}}_{\alpha,\beta,\omega})_y\frac{\partial U}{\partial y} + \frac{1}{\text{Re}}\Delta(\dot{\boldsymbol{\xi}}_{\alpha,\beta,\omega})_x$$

$$-i\omega\hat{v}_{\alpha,\beta,\omega} + i\alpha U_d\hat{v}_{\alpha,\beta,\omega} + \frac{\partial\hat{p}_{\alpha,\beta,\omega}}{\partial y} + \widetilde{D}(\hat{v}_{\alpha,\beta,\omega}) = \frac{1}{\text{Re}}\Delta(\dot{\boldsymbol{\xi}}_{\alpha,\beta,\omega})_y$$

$$-i\omega\hat{w}_{\alpha,\beta,\omega} + i\alpha U_d\hat{w}_{\alpha,\beta,\omega} + i\beta\hat{p}_{\alpha,\beta,\omega} + \widetilde{D}(\hat{w}_{\alpha,\beta,\omega}) = \frac{1}{\text{Re}}\Delta(\dot{\boldsymbol{\xi}}_{\alpha,\beta,\omega})_z$$

$$i\alpha\hat{u}_{\alpha,\beta,\omega} + \frac{\partial\hat{v}_{\alpha,\beta,\omega}}{\partial y} + i\beta\hat{w}_{\alpha,\beta,\omega} = 0; \quad \frac{\partial\sigma_{xy}}{\partial y} = \frac{\partial\sigma_{yy}}{\partial y} = \frac{\partial\sigma_{zy}}{\partial y} = 0, \tag{5}$$

with the modified diffusion operator

$$\widetilde{D}(\cdot) = -\frac{1}{\text{Re}}\left(-\alpha^2 + \frac{\partial^2 \cdot}{\partial y^2} - \beta^2\right) - \frac{1}{2}\left[-\alpha^2 a_{xx} + i\alpha a_{xy}\frac{\partial \cdot}{\partial y} - \alpha\beta a_{xz} + i\alpha\frac{\partial a_{yx}\cdot}{\partial y} + \frac{\partial}{\partial y}\left(a_{yy}\frac{\partial \cdot}{\partial y}\right)\right.$$

$$\left. + i\beta\frac{\partial a_{yz}\cdot}{\partial y} - \alpha\beta a_{zx} + i\beta a_{zy}\frac{\partial \cdot}{\partial y} - \beta^2 a_{zz}\right]. \tag{6}$$

The drift mean flow is $U_d(y) = U(y) - \frac{1}{2}\partial a_{xy}/\partial y$. The Fourier transform of $\boldsymbol{\sigma} d\boldsymbol{B}_t$ is noted $d\boldsymbol{\xi}_{\alpha,\beta,\omega}$, and the associated velocity Fourier component $\dot{\boldsymbol{\xi}}_{\alpha,\beta,\omega} = d\boldsymbol{\xi}_{\alpha,\beta,\omega}/dt$ is a standard centered Gaussian white noise convolved with the space-Fourier transform of $\boldsymbol{\sigma}$. As the mean flow is parallel, the random transport term of Eq. (4) reduces to $-(\dot{\boldsymbol{\xi}}_{\alpha,\beta,\omega})_y\partial U/\partial y$ in the right-hand side of Eq. (5), which is the strain induced by extraction of energy of the mean flow by the turbulence. This term is central in the lift-up mechanism [7] and it is the main actor in the role of incoherent turbulence in the streaks of streamwise velocity u. The choices of stochastic parameters $(\boldsymbol{\sigma}, \mathbf{a})$ are detailed in Sec. III D.

The main added-value of SLM in wall-bounded flows is to model the impact of time-decorrelated turbulence on the lift-up mechanism and its associated momentum mixing by stochastic diffusion. Due to stochastic transport, Eq. (5) is a stochastic equation for $\hat{\boldsymbol{u}}_{\alpha,\beta,\omega}$, Fourier transform of $\boldsymbol{u}'$. As a consequence, $\hat{\boldsymbol{u}}_{\alpha,\beta,\omega}$ is a random variable, whose variability will allow us to extract purely coherent components through the estimation of the CSD matrix $\mathbb{E}(\hat{\boldsymbol{u}}_{\alpha,\beta,\omega}\hat{\boldsymbol{u}}^*_{\alpha,\beta,\omega})$ and its eigenvectors. The leading eigenvector is called SLM. Our objective is to extract the dominant coherent component by

SLM, which is compared to the leading SPOD mode [58]. In Tissot *et al.* [41], ensemble method is employed for the estimation and we present in Sec. III C a reformulation of the problem as a singular value decomposition to improve computational efficiency.

B. Interactions between coherent structures

Equation (5) ensues from linearization of Eq. (4). Coming back to the ground assumptions in our stochastic modeling, a triple decomposition is performed on the displacement,

$$dX(x, t) = \bar{u}(x)dt + u'(x, t)dt + (\sigma dB_t)(x). \tag{7}$$

The first term $\bar{u}(x)dt = (U(y)\ 0\ 0)^T dt$ is the time-average displacement. The fluctuation is split in a time-differentiable component and an incoherent turbulent field, perceived as time decorrelated compared to the timescale of the coherent structure and modelled by a Brownian motion. Even if the time-average is nonambiguous, the splitting of the fluctuation is less obvious in general and is often performed through a phase or ensemble average operator [29,59]. The formulation (7) is a way to perform the triple decomposition in a unique manner through time differentiability of the variable (more precisely this decomposition is unique through the Bichteler-Dellacherie decomposition of stochastic processes [60]). Let us remark that the Brownian part σdB_t is modelled, while the time-differentiable part u' is solution of the system. Moreover, contrary to a splitting based on phase averaging, u' contains coherent and incoherent contributions.

With this decomposition in mind, it can be seen that the stochastic diffusion can be interpreted as a generalized eddy diffusion (since a full tensor **a** is involved) induced by the noise. In this case, the diffusion comes directly from the time decorrelation assumption and stems from the Itō-Wentzel formula, where Itō quadratic variations can be viewed as providing local averaging coefficients. The diffusion does not come from a Boussinesq hypothesis. This diffusion term accounts for the effect of time-decorrelated component and not for nonlinear interactions between time-differentiable components.

In system (5), the neglected term (written as a right-hand-side term in the momentum equation) is

$$\mathcal{F}(\overline{(u' \cdot \nabla)u'} - (u' \cdot \nabla)u'), \tag{8}$$

where $\mathcal{F}(\cdot)$ stands for space-time Fourier transform. As in resolvent analysis (presented in Supplemental Material [57]), this term is a convolution over all frequencies and wave numbers, which renders an explicit expression difficult to obtain. A major difference compared to ν-resolvent analysis is that it represents nonlinear interactions between smooth-in-time structures carrying coherent wave contributions and does not include time-decorrelated turbulent fluctuations. In that sense, its interpretation is closer to the forcing term in ν_t-resolvent analysis. We call the term (8) *wave-wave interactions*. The contribution of turbulent noise is already taken into account in the stochastic formulation.

We propose to treat the term (8) similarly to resolvent analysis and to model it as a Gaussian white noise forcing term. The addition of a forcing term to Eq. (5) leads to

$$
\begin{bmatrix}
-i\omega + i\alpha U_d + \widetilde{D}(\cdot) & \dfrac{\partial U}{\partial y} & 0 & i\alpha \\
0 & -i\omega + i\alpha U_d + \widetilde{D}(\cdot) & 0 & \dfrac{\partial \cdot}{\partial y} \\
0 & 0 & -i\omega + i\alpha U_d + \widetilde{D}(\cdot) & i\beta \\
i\alpha & \dfrac{\partial \cdot}{\partial y} & i\beta & 0
\end{bmatrix}
\begin{pmatrix}
\hat{u}_{\alpha,\beta,\omega} \\
\hat{v}_{\alpha,\beta,\omega} \\
\hat{w}_{\alpha,\beta,\omega} \\
\hat{p}_{\alpha,\beta,\omega}
\end{pmatrix}
$$

$$
=
\begin{bmatrix}
-(\dot{\xi}_{\alpha,\beta,\omega})_y \dfrac{\partial U}{\partial y} + \dfrac{1}{\mathrm{Re}}\Delta(\dot{\xi}_{\alpha,\beta,\omega})_x \\
\dfrac{1}{\mathrm{Re}}\Delta(\dot{\xi}_{\alpha,\beta,\omega})_y \\
\dfrac{1}{\mathrm{Re}}\Delta(\dot{\xi}_{\alpha,\beta,\omega})_z \\
0
\end{bmatrix}
+ b(y)
\begin{pmatrix}
\widetilde{f}_x^{NL} \\
\widetilde{f}_y^{NL} \\
\widetilde{f}_z^{NL} \\
0
\end{pmatrix}. \tag{9}
$$

The linear operator in the left-hand side of (9) can be written $\widetilde{\mathbf{A}}_{\alpha,\beta,\bar{q}} - i\omega\mathbf{E}$. The parameter $b(y)$ is an amplitude parameter of the nonlinear forcings whose choice is based on the turbulent fluctuation level observed in the data. Its choice is described in Sec. III D. The vector $(\widetilde{f}_x^{NL}, \widetilde{f}_y^{NL}, \widetilde{f}_z^{NL})^T$ carries independent standard centered Gaussian white noises. The above model will lead to forced stochastic linear modes, referred to as FSLM.

In system (9), two stochastic right-hand-side terms come from distinct physical mechanisms: The first term function of $\dot{\boldsymbol{\xi}}_{\alpha,\beta,\omega}$ is related to stochastic transport by incoherent small-scale turbulence, while the second forcing term accounts for the nonlinear interactions between coherent structures.

C. Numerical computation of the forced stochastic linear modes formalism

In Tissot *et al.* [41], an ensemble of solutions are computed to obtain an empirical CSD matrix. This procedure turns out to be more expensive than a SVD for small size problems (one-dimensional in the y direction). We can note that for large-scale problems, advanced ensemble-based techniques [61,62] or time-domain formulations [63] can be employed. We propose here to write FSLM as an SVD problem. Starting from system (9) and similarly as in resolvent analysis (presented in the Supplemental Material [57]), we define

$$\widetilde{\mathbf{L}}_{\alpha,\beta,\omega} = \mathbf{H}(\widetilde{\mathbf{A}}_{\alpha,\beta,\bar{q}} - i\omega\mathbf{E})^{-1}\widetilde{\mathbf{B}}, \tag{10}$$

with

$$\mathbf{H} = \begin{pmatrix} \mathbb{I} & 0 & 0 & 0 \\ 0 & \mathbb{I} & 0 & 0 \\ 0 & 0 & \mathbb{I} & 0 \end{pmatrix}, \quad \widetilde{\mathbf{B}} = \begin{bmatrix} -(\boldsymbol{\Phi}^\sigma)_y\mathbb{D}^\sigma\frac{\partial U}{\partial y} + \frac{1}{\text{Re}}\Delta(\boldsymbol{\Phi}^\sigma)_x\mathbb{D}^\sigma & b(y)\mathbb{I} & 0 & 0 \\ \frac{1}{\text{Re}}\Delta(\boldsymbol{\Phi}^\sigma)_y\mathbb{D}^\sigma & 0 & b(y)\mathbb{I} & 0 \\ \frac{1}{\text{Re}}\Delta(\boldsymbol{\Phi}^\sigma)_z\mathbb{D}^\sigma & 0 & 0 & b(y)\mathbb{I} \\ 0 & 0 & 0 & 0 \end{bmatrix}, \tag{11}$$

with $\mathbb{I}$ the identity matrix. The output operator $\mathbf{H}$ specifies that the modes will be optimal in terms of kinetic energy. The input operator $\widetilde{\mathbf{B}}$ maps the vector of random variables

$$\widetilde{\boldsymbol{f}} = (\eta_1, \ldots, \eta_{N_\sigma}, \widetilde{f}_x^{NL}, \widetilde{f}_y^{NL}, \widetilde{f}_z^{NL})^T$$

to the forcing space of the linearized system. The matrix $(\boldsymbol{\Phi}^\sigma)_j$, for $j = \{x, y, z\}$, gathers in columns $(\boldsymbol{\Phi}_k^\sigma)_j$ for $k \in [1, N_\sigma]$, an expansion basis of the noise $d\boldsymbol{\xi}_{\alpha,\beta,\omega} = \sum_{k=1}^{N_\sigma} c_k \boldsymbol{\Phi}_k^\sigma \eta_k$ which will be specified in Sec. III D, with η_k standard centered Gaussian white noises. The diagonal matrix $\mathbb{D}^\sigma$ contains the associated amplitude coefficients c_k.

We perform the singular value decomposition

$$\mathbf{W}^{\frac{1}{2}}\mathbf{H}(\widetilde{\mathbf{A}}_{\alpha,\beta,\bar{q}} - i\omega\mathbf{E})^{-1}\widetilde{\mathbf{B}}\mathbf{W}_f^{-\frac{1}{2}} = \mathbf{U}_{\text{FSLM}}\boldsymbol{\Sigma}_{\text{FSLM}}\mathbf{V}_{\text{FSLM}}^*, \tag{12}$$

with

$$\mathbf{W}_f = \begin{pmatrix} \mathbb{I} & 0 \\ 0 & \mathbf{W} \end{pmatrix}. \tag{13}$$

As a final step, FSLM are defined by $\boldsymbol{\Phi}_i^{\text{FSLM}} = \mathbf{W}^{-\frac{1}{2}}V_{\text{FSLM},i}$, where the first mode is the predicted coherent structure and the higher-order modes are used to define the noise at the next iteration (see Sec. III D). Moreover, as in resolvent analysis, an estimation of the CSD matrix can be obtained by $\mathbf{S} = \widetilde{\mathbf{L}}_{\alpha,\beta,\omega}\widetilde{\mathbf{L}}_{\alpha,\beta,\omega}^*$.

D. Choice of parameters in FSLM

We recall that we focus on coherent structures perturbed by turbulent flows in the buffer and logarithmic layers at scales where production exceeds dissipation, for which, therefore, a forward energy cascade is expected [35]. In the logarithmic layer, we focus on energetic scales, and as

highlighted in Jiménez [64], dissipation takes place at a smaller scale. We expect in this region an energy cascade draining energy from large to small scales through an interscale energy flux. For large energetic scales in the logarithmic layer, we expect as well a larger influence of incoherent turbulence onto the wave compared to the buffer layer; we aim at modeling such influence by FSLM.

The two-point statistics of the noise, carried by $\boldsymbol{\sigma}$, have to represent time decorrelated turbulent velocity field fluctuations. Its definition is an open question and relies on *a priori* knowledge of the fluctuating velocity field. Our strategy is to use few parameters, preferably with quantities available in standard simulation data or well documented in the literature. Moreover, we need to respect the ground hypothesis that the noise is decorrelated from resolved coherent field (at the large-scale characteristic timescale).

We propose to set the variance tensor, $\mathbf{a}$, defined in Eq. (3), from root-mean-square (RMS) velocity profiles, and variances of velocity fluctuations, which are quantities often available in databases accompanying the mean flow profile:

$$\mathbf{a}(y) = \tau_s \begin{bmatrix} \langle u'^2(y) \rangle & \langle u'(y)v'(y) \rangle & 0 \\ \langle u'(y)v'(y) \rangle & \langle v'^2(y) \rangle & 0 \\ 0 & 0 & \langle w'^2(y) \rangle \end{bmatrix}, \tag{14}$$

where $\langle \cdot \rangle$ denotes average in time and in the homogeneous directions. The underlying hypothesis to use RMS profiles is that the contribution of the single coherent wave we are trying to predict is small compared to the whole time-domain solution. Thus, the RMS, which contains all contributions of the turbulent velocity field is a fair estimate of the turbulence which impacts the wave. The decorrelation time τ_s, necessary for dimensional consistency, represents the timescale necessary for the Brownian motion to perform mixing by stochastic diffusion. This parameter is crucial for obtaining relevant results since it controls the level of diffusion. The timescale τ_s should represent, at a given wavelength, the timescale necessary for the turbulence to affect the wave by a transport mechanism. For this, we rely on an inertial scaling $\tau_s = \tau_0 (l/l_0)^{\frac{2}{3}}$ proposed in Ref. [65], assuming that the wavelength lies within the inertial range of an energy cascade under Kolmogorov hypotheses and that this turbulent field is incoherent with the wave solution. The time $\tau_0 = l_0/U_0$ is the outer timescale, $l_0 = 2$ is the channel height, U_0 is the velocity averaged over the wall-normal direction; the scale of the wave is $l = 2\pi/\sqrt{k_x^2 + k_z^2}$ with $k_x = 2\pi/\lambda_x$ and $k_z = 2\pi/\lambda_z$ [10]. This scaling is valid for scales such that $l < l_0$. We do not expect our scaling to be valid for l larger than the channel height leading to structures living in the outer region. It can be noticed that the structure of the model allows a scale-dependent stochastic diffusion through the decorrelation time τ_s, which is set here by a physical scaling. In Gupta *et al.* [38], a similar scale dependence of the eddy diffusion has been observed to be necessary to produce accurate results.

The noise $d\boldsymbol{\xi}_{\alpha,\beta,\omega}$ is the space-time Fourier transform of $\boldsymbol{\sigma}d\boldsymbol{B}_t$. It is white in time, and its covariance is the CSD of $\boldsymbol{\sigma}d\boldsymbol{B}_t$. It should match the Fourier transform of the cross-correlation tensor of $\boldsymbol{\sigma}d\boldsymbol{B}_t$, whose diagonal is the variance tensor $\mathbf{a}$. Indeed, the cross-spectral density of $\boldsymbol{\sigma}d\boldsymbol{B}_t$ is

$$\mathbb{E}\big(d\xi_{\alpha,\beta,\omega}^i \big(d\xi_{\alpha,\beta,\omega}^j\big)^H\big) = \mathcal{F}\big(\mathbb{E}\big((\boldsymbol{\sigma}d\boldsymbol{B}_t)_x^i (\boldsymbol{\sigma}d\boldsymbol{B}_{t'})_{x'}^j\big)\big), \tag{15}$$

and we recall the link with the variance tensor $\mathbf{a}$ in Eq. (3). As a consequence, defining the noise based on an expansion onto SPOD modes $\boldsymbol{\Phi}_k^{\text{SPOD}}$ associated with the eigenvalues λ_k^{SPOD},

$$d\boldsymbol{\xi}_{\alpha,\beta,\omega} = \sum_{k=1}^{\infty} \sqrt{\lambda_k^{\text{SPOD}}} \, \boldsymbol{\Phi}_k^{\text{SPOD}} \eta_k, \tag{16}$$

with η_k standard centered Gaussian white noise variables, is consistent with the definition of $\mathbf{a}$ in Eq. (14), since SPOD modes are eigenfunctions of the CSD matrix of the turbulent fluctuation. This definition has two main issues. The first is the requirement of a fine description of the turbulent velocity field, since SPOD modes are required. Instead, we aim at constructing a model with a reduced quantity of data. The second issue is that in definition (16), the FSLM coherent structure

Algorithm 1. Iterative procedure for FSLM.

Compute ν-resolvent: $\mapsto (s^{\nu-\text{resolvent}}, \mathbf{\Phi}^{\nu-\text{resolvent}})$

$\mathbf{\Phi}_k^{\sigma,(1)} \leftarrow \mathbf{\Phi}_{k+1}^{\nu-\text{resolvent}}, c_k^{(1)} = s_{k+1}^{\nu-\text{resolvent}} \frac{\sqrt{\lambda_1^{\text{SPOD}}}}{s_1^{\nu-\text{resolvent}}}, \mathbf{S}^{(1)} \leftarrow \sum_{k=0}^{N_\sigma} \left(c_k^{(1)}\right)^2 \mathbf{\Phi}_k^{\sigma,(1)} \mathbf{\Phi}_k^{\sigma,(1)*};$

$n \leftarrow 1;$

while *not converged* **do**

   Compute FSLM by SVD procedure (sec. III C): $\mapsto (\widetilde{L}_{\alpha,\beta,\omega}, \lambda^{\text{FSLM}}, \mathbf{\Phi}^{\text{FSLM}});$

   $\mathbf{S}^{(n+1)} \leftarrow \widetilde{L}_{\alpha,\beta,\omega} \widetilde{L}_{\alpha,\beta,\omega}^*;$

   $\mathbf{\Phi}_k^{\sigma,(n+1)} \leftarrow \mathbf{\Phi}_{k+1}^{\text{FSLM}}, c_k^{(n+1)} \leftarrow \sqrt{\lambda_{k+1}^{\text{FSLM}}};$

   if $\|\mathbf{S}^{(n+1)} - \mathbf{S}^{(n)}\|_F / \|\mathbf{S}^{(1)}\|_F < \epsilon$ **then**

      converged $\leftarrow True;$

   end

end

---

would be necessarily correlated with a part of the noise, since it would be spanned by the full SPOD basis. Ultimately, we would like to subtract it from the noise basis, but only at the considered frequency-wave-number couple to not invalidate our definition (14).

To address these issues, we propose to relax the strong consistency between Eq. (16) and the diffusion tensor **a** Eq. (14). Instead, we ensure that the noise is decorrelated from the wave by modifying the definition of the noise. First, we express it as an expansion onto an orthonormal basis

$$d\boldsymbol{\xi}_{\alpha,\beta,\omega} = \sum_{k=1}^{N_\sigma} c_k \, \mathbf{\Phi}_k^\sigma \, \eta_k. \tag{17}$$

We then propose a first guess by defining $\mathbf{\Phi}_k^\sigma = \mathbf{\Phi}_{k+1}^{\nu-\text{resolvent}}$ and $c_k = \sqrt{\lambda_1^{\text{SPOD}}} s_{k+1}^{\nu-\text{resolvent}} / s_1^{\nu-\text{resolvent}}$, with $k \in [1, \ldots, N_\sigma]$, $(s_k^{\nu-\text{resolvent}}, \mathbf{\Phi}_k^{\nu-\text{resolvent}})$ the kth singular value and optimal response mode of ν-resolvent analysis and λ_1^{SPOD} the first SPOD eigenvalue. This guess rescales the noise spanned by ν-resolvent suboptimal modes in such a way that the energy of the first mode matches the first SPOD mode. Doing this, we define an orthonormal family of vectors orthogonal to the dominant resolvent mode. The amplitude rescaling aims at obtaining a rough approximate consistency between $\boldsymbol{\sigma}$ and the definition of **a** by the RMS profiles. The use of resolvent modes as a first guess frees the modeling from the data. Only the first SPOD eigenvalue is required, but this single parameter can be replaced by a free parameter fixed by some physical knowledge to obtain a full model-based procedure, in which no data is required.

In a second step, we correct the definition of (17) in order to ensure that the noise is decorrelated from the first FSLM. Once expressed in the Fourier domain, the time decorrelation becomes a decorrelation between ensemble realizations of the Fourier component. As explained in Towne *et al.* [58] for the SPOD modes, since the CSD matrix has been diagonalized, the contribution of separate eigenfunctions are decorrelated. We then construct a noise spanned by the eigenfunctions of the CSD matrix excluding the first FSLM. For that, we choose $\mathbf{\Phi}_k^\sigma = \mathbf{\Phi}_{k+1}^{\text{FSLM}}$ and $c_k = \sqrt{\lambda_{k+1}^{\text{FSLM}}}$, with $k \in [1, \ldots, N_\sigma]$, where $(\lambda_k^{\text{FSLM}}, \mathbf{\Phi}_k^{\text{FSLM}})$ are eigenelements of CSD matrix **S** of FSLM solutions. The procedure is cyclic since high-order modes of FSLM are mandatory to predict the leading FSLM mode, but it is possible to compute it iteratively through a fixed point procedure initialized with the first guess, as summarized in Algorithm 1. In practice, calculations converge quickly in few (less than 10) iterations with a relative tolerance on the Frobenius norm $\| \cdot \|_F$ of the CSD equal to $\epsilon = 10^{-3}$. An example of convergence is shown in the Supplemental Material [57]. It can be noticed in particular that it converges toward a solution where the energy decay of the spectrum is similar to SPOD (see Sec. IV D), which does not invalidate the consistency between noise and stochastic diffusion. Moreover, the decay in the singular values is moderately fast suggesting an incoherent

TABLE I. Numerical parameters for the simulations.

Re_τ	Re	N_x	N_y	N_z	Δx^+	Δy_{min}^+	Δy_{max}^+	Δz^+	Δt^+
180 (179)	2800	192	129	192	11.7	5.4×10^{-2}	4.4	5.9	5.7
550 (543)	10 000	384	257	384	8.9	4.1×10^{-2}	6.7	4.4	3.0
1000 (996)	20 000	484	385	484	12.9	3.3×10^{-2}	8.2	6.5	2.5

(by construction) contribution that is sufficiently small to be considered as a noise but too large to be neglected.

To summarize, the proposed procedure uses the RMS profiles to define the diffusion tensor **a**, which is the one defined in the time-domain in Eq. (3). The noise $d\boldsymbol{\xi}_{\alpha,\beta,\omega}$, the space-time Fourier transform of $\boldsymbol{\sigma} d\boldsymbol{B}_t$, is expanded on an orthonormal basis, which is estimated by an iterative procedure ensuring decorrelation between the noise and the solution. An initial guess is defined by resolvent modes rescaled using the first SPOD eigenvalue in order to obtain consistency with the definition of **a** with a minimum of data.

Finally, in FSLM, the nonlinear forcing amplitude has to be given. In order to obtain a physically relevant order of magnitude, the nonlinear forcing amplitude $b(y)$ is chosen as $(\sqrt{\lambda_1^{\mathrm{SPOD}}}/s_1^{\nu-\mathrm{resolvent}})[\mathrm{TKE}(y)/\max(\mathrm{TKE})]$, with $\mathrm{TKE}(y) = \langle u'^2 \rangle + \langle v'^2 \rangle + \langle w'^2 \rangle$ the turbulent kinetic energy. This scaling allows us to define a profile of nonlinear forcing in the wall-normal direction consistent with the turbulent activity and such that the response of the deterministic linearized system (without eddy viscosity) to this forcing has an amplitude comparable with SPOD.

IV. APPLICATION TO TURBULENT CHANNEL FLOW

A. Numerical simulation

Databases of direct numerical simulation of turbulent channels were obtained with the pseudospectral code Channelflow 2.0 [66]. Periodic boundary conditions are enforced in the streamwise (x) and spanwise (z) directions and Chebyshev polynomials are used in the wall-normal direction (y). Parameters are given in Table I and additional numerical details, including validation results, can be found in Amaral *et al.* [24]. Mean flow profiles for the three Reynolds numbers and RMS profiles at $Re_\tau = 1000$ are presented in Fig. 1. Results are presented using nondimensional quantities using viscous (wall) scaling, denoted with a + superscript.

SPOD has been computed as a reference to which ν_t-resolvent analysis and FSLM will be compared. They represent the most energetic structure for a given frequency-wave-number
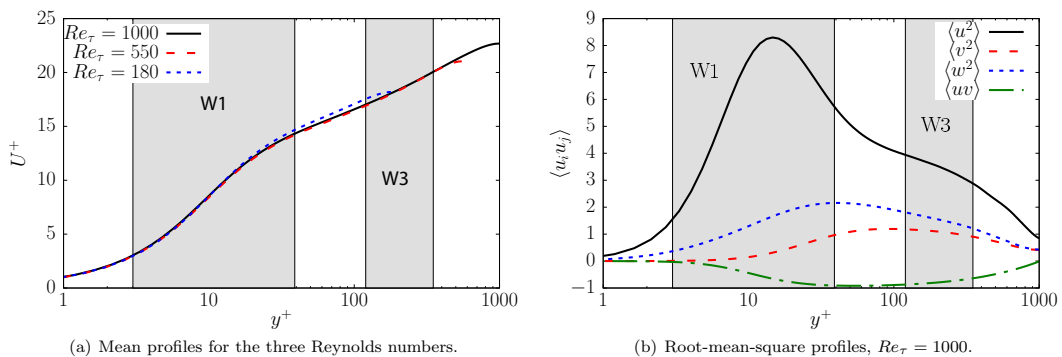

(a) Mean profiles for the three Reynolds numbers.

(b) Root-mean-square profiles, $Re_\tau = 1000$.

FIG. 1. Mean and root-mean-square profiles. Gray areas indicate the spatial supports of W1 and W3.

(a) Mean velocity (plain black line) and mean velocity with the corrective drift associated with W1 to W4 at $Re_\tau = 1000$ (see Supplementary Material [57] for W2 and W4).

(b) Schematic representation of the drift velocity effect of the term $-\frac{1}{2}\frac{\partial a_{xy}}{\partial z}$.
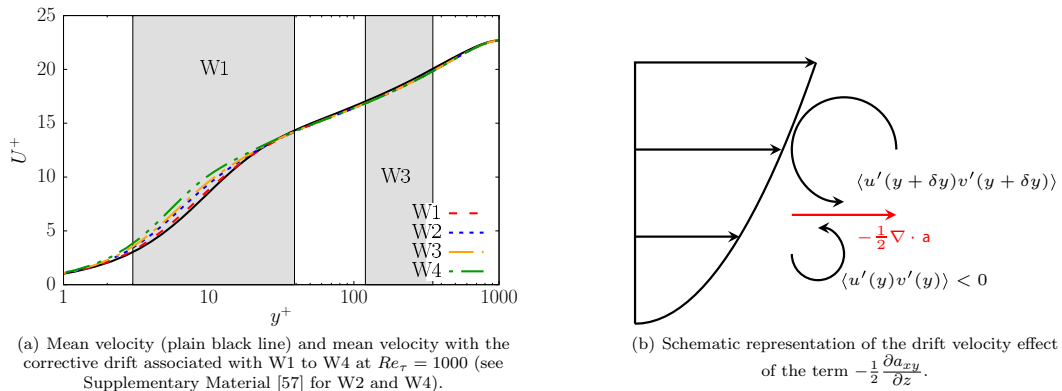
FIG. 2. Effect of the drift velocity.

combination, which can be meaningfully compared to most amplified responses of resolvent and FSLM. Complementary numerical details are given in Supplemental Material [57].

Resolvent modes are known [19,61] to show large responses around the critical layer y_c^+, i.e., where the phase speed $c^+ = \lambda_x^+/\lambda_t^+$ matches the mean flow $U^+(y_c^+)$. SPOD modes follow the same trend, which is consistent with the fact that these modes are equivalent if the nonlinear term behaves as a Gaussian white noise [67]. Two waves have been selected: one denoted W1 with $(\lambda_x^+, \lambda_z^+, \lambda_t^+) \approx (1000, 100, 100)$, typical of the streaks structures in the buffer layer chosen at the lowest Reynolds number $Re_\tau = 180$, and one denoted W3 with $(\lambda_x^+, \lambda_z^+, \lambda_t^+) \approx (2000, 500, 100)$, evolving within the logarithmic layer at the highest Reynolds number $Re_\tau = 1000$. In Supplemental Material [57], numerical details are presented. Moreover, the robustness of the method is shown by varying Reynolds number for W1, and two other waves (W2 and W4) are presented in order to vary the wall distance of the wave spatial support. As in Tissot *et al.* [41] we consider modes that are odd in u and w (and thus even in v) around the channel centerline. This has been performed by enforcing symmetry in the operators $\mathbf{L}_{\alpha,\beta\omega}$, $\mathbf{H}$, $\widetilde{\mathbf{B}}$.

The spatial supports of the waves W1 and W3 are reported in Fig. 1. In Fig. 2(a), the drift velocity (in wall units) associated with W1 to W4 are displayed at $Re_\tau = 1000$. It shows that the corrective drift $-\frac{1}{2}\partial a_{xy}/\partial y$ plays essentially a role in the buffer region. Since the variance tensor $\mathbf{a}$ is defined based on RMS profiles in Eq. (14), the drift velocity accounts for the effective transport induced by the wall-normal variations of $\langle u'(y)v'(y)\rangle$. In the buffer region, the magnitude of $\langle u'v'\rangle$ (with negative values) increases with the wall distance, and this inhomogeneity tends to induce a positive streamwise transport velocity, which corresponds to the corrective drift term $-\frac{1}{2}\partial a_{xy}/\partial y$. This effective transport by the turbulent fluctuations is taken into account in the proposed linearized model and does not appear explicitly in an eddy-viscosity model. This relevance of the drift velocity in the buffer region is in line with the observations and modeling of Pinier *et al.* [50]. Additionally, we can see that with our definition, the effect of drift velocity is more pronounced for waves evolving at higher wall-normal distance due to larger decorrelation times τ_s. As a matter of fact, for such long waves there is a more substantial contribution of the stochastic transport, which occurs with a longer decorrelation time.

B. Buffer layer

In the buffer layer, we present the results at $Re_\tau = 180$, and complementary results at $Re_\tau = 550$ and $Re_\tau = 1000$ are given in the Supplemental Material [57]. Figure 3(a) shows a velocity field cross section of the SPOD for W1 ($\lambda_x^+ = 1124$, $\lambda_z^+ = 102$, $\lambda_t^+ = 100$). It shows a typical streaky structure of u with streamwise vortices (rolls), which highlights the lift-up mechanism: In regions of high streamwise velocity high-speed streak are emerging. They are associated with negative
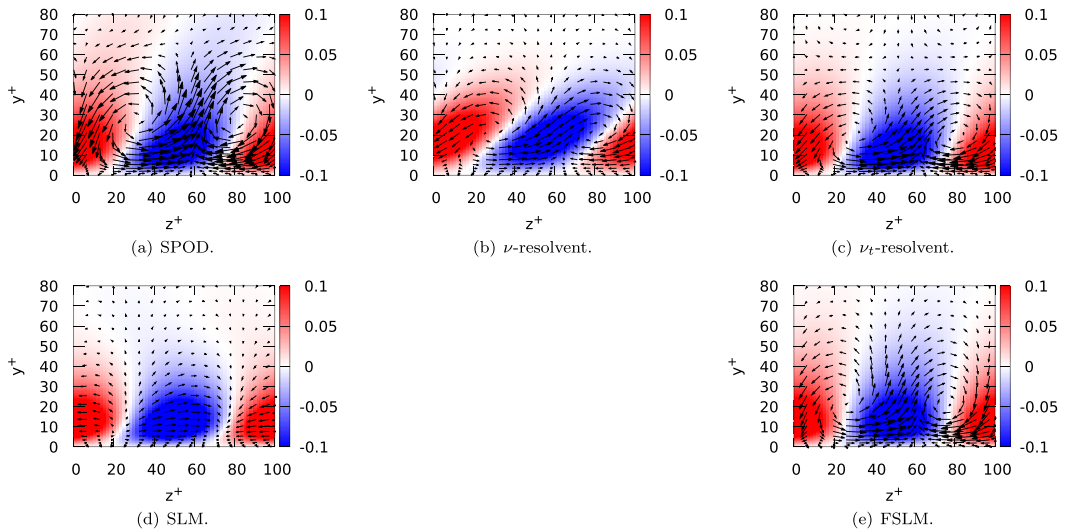
FIG. 3. Reconstructions of W1 at $Re_\tau = 180$. Colors are streamwise velocities, arrows are in-plane velocity fields.
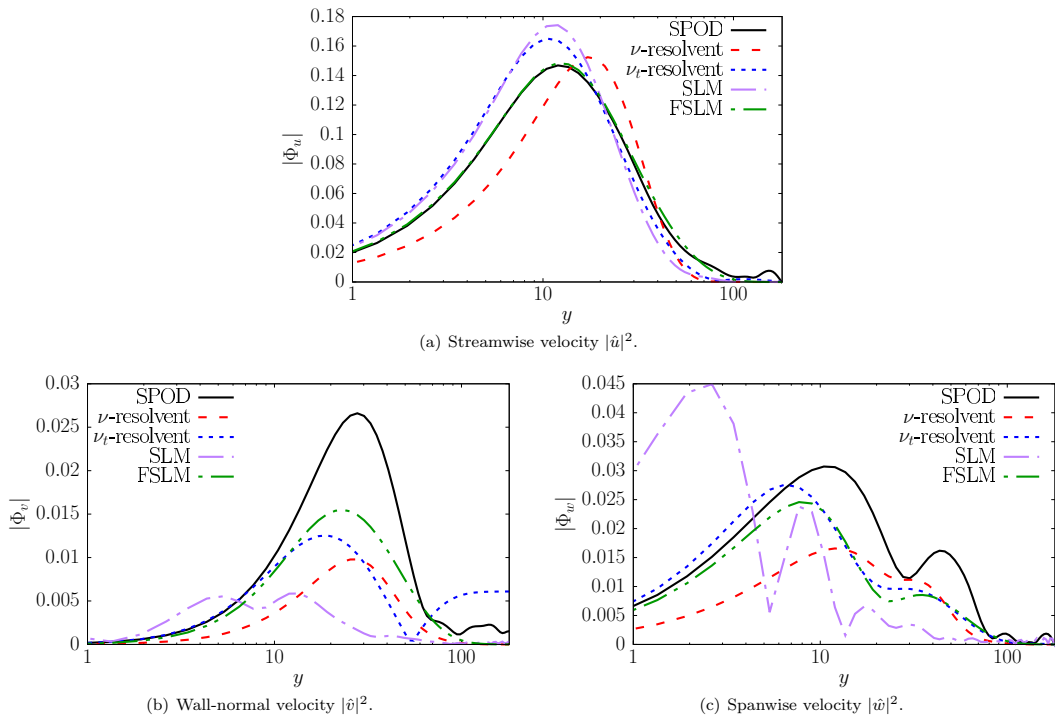
v components, which transport fluid with high streamwise velocity to a region with lower mean flow; the opposite happens for low-speed streaks, which are associated with positive v components. Predictions by v-resolvent and v_t-resolvent analysis are shown in Figs. 3(b) and 3(c), respectively. We can see a relevant prediction, with an improvement when eddy viscosity is added. This is consistent with Morra *et al.* [32]. Figure 3(d) shows the solution of the proposed stochastic model but omitting the nonlinear forcing (SLM). It can be seen that the streaks are well predicted, but the rolls are absent. However, taking into account wave-wave interactions by a nonlinear forcing (FSLM) enables us to recover the rolls and to obtain accurate predictions. This can be explained by the fact that stochastic transport models the effect of the incoherent part of the velocity field, thus leading to good predictions of the u profiles. Since near-wall streamwise vortices are thought to arise from a nonlinear interaction of coherent structures [5], a nonlinear forcing is mandatory to predict them. Resolvent analysis with eddy viscosity leads to good predictions as it takes into account this nonlinear forcing and incorporates eddy diffusion. These predictions are significantly enhanced by the stochastic model since it explicitly modifies lift-up by incoherent turbulent motions through three complementary terms: the transport by the noise, a diffusion tensor with nonzero off-diagonal terms and a drift velocity active in the buffer region [41].

Profiles of power spectral density (PSD) of the three velocity components are shown in Fig. 4. They confirm that streamwise velocity (u) profiles are similarly captured by v_t-resolvent and by SLM. The agreement of FSLM with SPOD data is significantly improved. Moreover, the streamwise vortices signing on the (v, w) profiles are not captured by SLM but strongly intensified in FSLM. The wall-normal velocity (v) is especially affected by the stochastic transport leading to the best agreement with SPOD.

To demonstrate the robustness of the procedure, buffer layer modes at other Reynolds numbers are shown in Supplemental Material [57]. Despite a slight overall deterioration of agreement between all models and SPOD when the Reynolds number increases, the trend is maintained and FSLM shows systematically a better agreement.

C. Logarithmic layer

We now select a wave named W3 evolving within the logarithmic layer by setting the phase speed $c^+ = 18.1$ associated with a critical level $y_c^+ = 180$. The wave-number ($\lambda_x^+ = 2087$, $\lambda_z^+ = 522$) has

(a) Streamwise velocity $|\hat{u}|^2$.

(b) Wall-normal velocity $|\hat{v}|^2$.

(c) Spanwise velocity $|\hat{w}|^2$.

FIG. 4. PSD velocity profiles of W1 at $\mathrm{Re}_\tau = 180$.

been chosen in the energy peak (taken from Ref. [24]) of the premultiplied powerspectra of the streamwise velocity. It can be extracted by SPOD, as shown in Fig. 5(a). The ν-resolvent analysis [Fig. 5(b)] extracts typical critical layer modes, with a narrow spatial support located at the critical layer, i.e., at the wall-normal position y_c^+ where the phase speed c^+ matches the mean velocity. Incorporating eddy viscosity [Fig. 5(c)] leads to wider spatial support, more similar to SPOD modes, which is again consistent with previous studies [32]. However, there is room for improvements, since SPOD modes show a structure that peaks further from the wall than what is predicted by ν_t-resolvent. FSLM in Fig. 5(d) improves significantly this prediction with the streamwise velocity structure further from the wall and a more accurate shape of the rolls.

Figure 6 showing the PSD profiles highlights quantitatively this improvement. Concerning the u component, Fig. 6(a) shows that differently from the other models, the spatial support is very well captured. As for the wall-normal v velocity, the shape of the profile is better predicted but with a high relative amplitude. The spanwise w velocity is better captured as well.

The lower accuracy of ν_t-resolvent predictions can be understood by the fact that the effect of the incoherent turbulent field on the wave is modelled only by a diffusive mechanism. On the contrary, FSLM incorporates through stochastic transport some driving mechanisms induced by the incoherent motions existing at the same scale. The success of FSLM suggests that in the logarithmic region, where the turbulence is developed, taking into account the stochastic nature of the log-layer structures is central to perform accurate predictions.
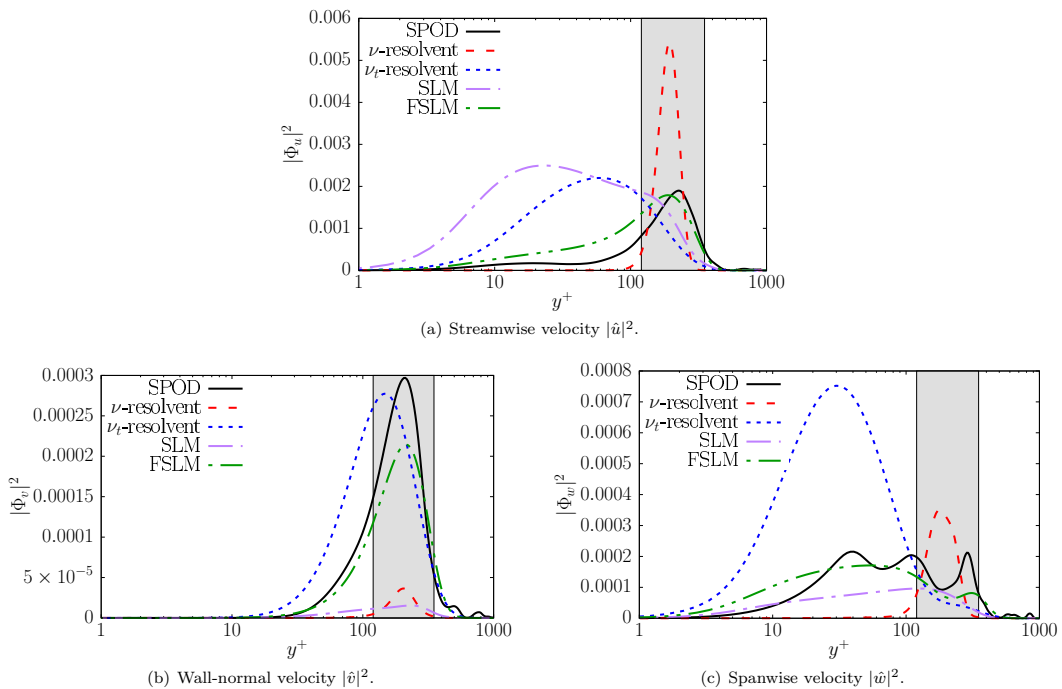
In addition, profiles of SLM, i.e., neglecting the nonlinear forcing, are shown to produce poor predictions. This suggests again that coherent nonlinear wave-wave interactions are crucial for self-sustaining process for log-layer. It corroborates hypotheses in Flores and Jiménez [8] and Cossu and Hwang [12] that a coherent large-scale self-sustaining process is in action for large log-layer structures.

(a) SPOD.

(b) ν-resolvent.

(c) ν_t-resolvent.

(d) FSLM.
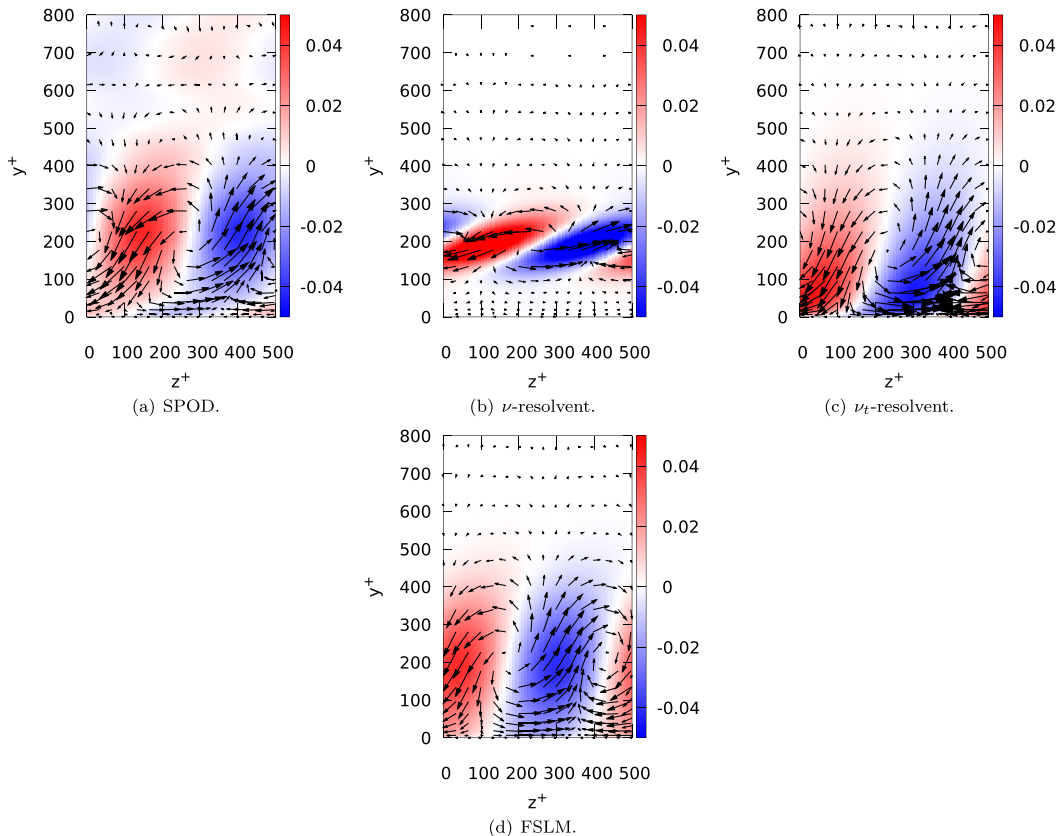
FIG. 5. Reconstructions of W3 at $Re_\tau = 1000$.

Frequency-wave-number space has been swept, and colinearity metrics

$$\theta_{\alpha,\beta,\omega}^{\text{model}} = \frac{\left|\left(\boldsymbol{\Phi}_{1,\alpha,\beta,\omega}^{\text{model}}, \boldsymbol{\Phi}_{1,\alpha,\beta,\omega}^{\text{SPOD}}\right)\right|}{\left\|\boldsymbol{\Phi}_{1,\alpha,\beta,\omega}^{\text{model}}\right\| \left\|\boldsymbol{\Phi}_{1,\alpha,\beta,\omega}^{\text{SPOD}}\right\|}, \tag{18}$$

have been computed (metric used for instance in Ref. [68]). This metric is a normalized inner product between the dominant SPOD mode $\boldsymbol{\Phi}_{1,\alpha,\beta,\omega}^{\text{SPOD}}$ and the mode issued from a given model $\boldsymbol{\Phi}_{1,\alpha,\beta,\omega}^{\text{model}}$. A value of 1 means exact colinearity between modes, while 0 happens when the modes are orthogonal. Then, we compute the metric $\gamma_{\alpha,\beta,\omega} = \log(\theta_{\alpha,\beta,\omega}^{\text{FSLM}}/\theta_{\alpha,\beta,\omega}^{\nu_t\text{-resolvent}})$, which represents the improvement ($\gamma > 0$) or deterioration ($\gamma < 0$) of colinearity with SPOD compared to the ν_t-resolvent model. Figure 7 shows the value of $\gamma_{\alpha,\beta,\omega}$ at four critical layer positions as a function of streamwise and spanwise wave numbers. We can see that in the buffer and logarithmic layer, a wide range of streamwise elongated structures are improved with FSLM compared to ν_t-resolvent analysis. The improvement is more pronounced further from the wall since agreement is more difficult to obtain. Complementary maps of $\theta_{\alpha,\beta,\omega}^{\text{model}}$ are given in the Supplemental Material [57]. Isocontour of the premultiplied first SPOD eigenvalue $\alpha\beta\lambda_1^{\text{SPOD}}$ are superimposed and show that deterioration happens at scales where less energy is present. Finally, in Fig. 7(d) almost in the outer region, we can see that FSLM provide slightly worse performances than ν_t-resolvent for large λ_x and λ_z. We explain this discrepancy by the choice of decorrelation time τ_s, which is designed based on inertial-range scalings (see Sec. III D). These maps prove a wide range of validity of the proposed model.

(a) Streamwise velocity $|\hat{u}|^2$.

(b) Wall-normal velocity $|\hat{v}|^2$.

(c) Spanwise velocity $|\hat{w}|^2$.

FIG. 6. PSD velocity profiles of W3 at $\mathrm{Re}_\tau = 1000$.

D. Eigenspectrum

In Fig. 8, we compare the eigenvalues λ^{FSLM} of the FSLM model, i.e., the eigenvalues of $\mathbf{S}^{(n)}$ once the iterative procedure is converged, with the SPOD eigenvalues. It is performed for the two examples $W1$ at $\mathrm{Re}_\tau = 550$ and $W3$ at $\mathrm{Re}_\tau = 1000$. As a reference, we show the spectrum of ν-resolvent amplification energy gain $(\sigma^{\nu-\mathrm{resolvent}})^2$, which constitutes the initial guess of the iterative procedure. It can be seen that even if the initial guess has a spectrum with a decay that is too fast, the iterative procedure succeeds to produce a rate of energy decay similar to SPOD. We recall that these values have not been informed in the model, and it is only a consequence of the constraint that the noise is decorrelated from the FSLM coherent structure. We recall that a noise based on an expansion onto SPOD ensures consistency between the noise expressed in the Fourier domain and the definition given to the stochastic diffusion using RMS profiles. The fact that we recover a spectrum similar to SPOD suggests that the incoherent field spanned by suboptimal is relevant, despite the relaxation of the strong consistency between SPOD and RMS profile. Moreover, the moderate decay in the spectrum indicates that, after convergence, the incoherent part cannot be neglected.

As an indication, we have also shown in Fig. 8 the energy gain spectrum of ν_t-resolvent analysis. Consistently with the observations in Ref. [36], in the energetic scales of the buffer layer the energy gain of suboptimal modes of ν_t-resolvent analysis decays as fast as in ν-resolvent analysis, with a strongly low-rank behavior. However, in the log-layer, adding eddy-viscosity reduces this low-rank behavior, and we can see in Fig. 8 that it rejoins the decay rate of SPOD. FSLM has a decay rate of the spectrum close to SPOD in both cases.

As a caveat, we recall that the comparison is made with a specific eddy viscosity model, which has been adjusted in Del Álamo and Jiménez [69] to match the numerical mean flow at $\mathrm{Re}_\tau = 2000$. It may be highlighted that this eddy viscosity is not necessarily optimal for all Reynolds numbers. Moreover, the eddy viscosity designed to match the mean flow is also not necessarily optimal to
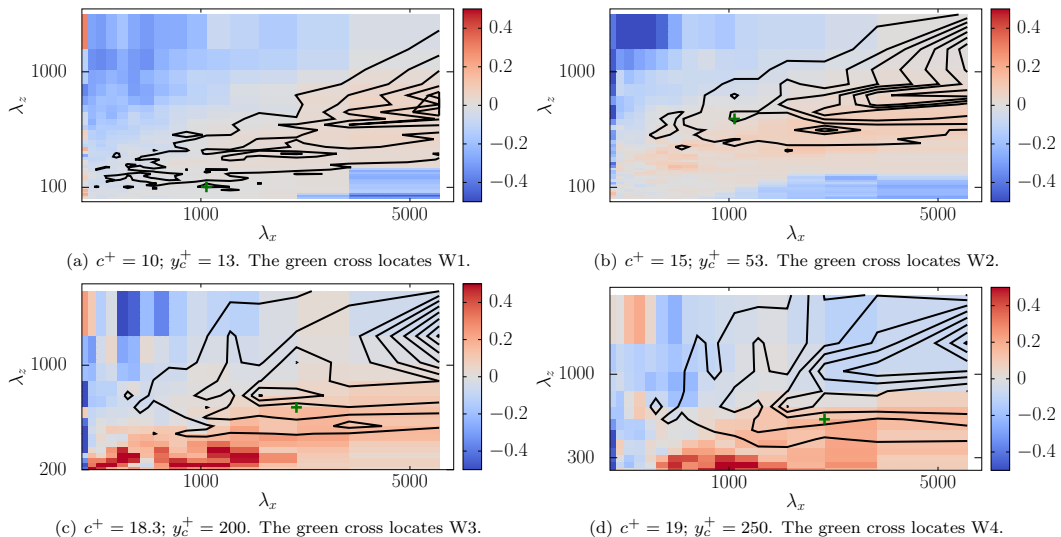
(a) $c^+ = 10$; $y_c^+ = 13$. The green cross locates W1.

(b) $c^+ = 15$; $y_c^+ = 53$. The green cross locates W2.

(c) $c^+ = 18.3$; $y_c^+ = 200$. The green cross locates W3.

(d) $c^+ = 19$; $y_c^+ = 250$. The green cross locates W4.

FIG. 7. Metric $\gamma_{\alpha,\beta,\omega} = \log(\theta_{\text{FSLM}}/\theta_{\nu_t\text{-res}})$ of improvement (>0) or deterioration (<0) of collinearity between FSLM and SPOD compared to ν_t-resolvent analysis as a function of λ_x, λ_z for various critical layer positions. Isocontours are the premultiplied value of the first SPOD $\alpha\beta\lambda_1^{\text{SPOD}}$.

predict a coherent structure at a given wave number–frequency couple. There are, indeed, some indications in the literature that the eddy viscosity should be dependent on the wave number [36,38]. On the other hand, the FSLM incorporates as well a given amount of data, but no optimization procedure to match data. A fully consistent comparison is not obvious, and we keep in mind that some amount of improvement could be obtained as well in ν_t-resolvent analysis by optimizing an eddy viscosity parameter. The goal is here more to highlight the benefit of stochastic modeling under location uncertainty than putting models in competition.

V. MODELLING RECOMMENDATIONS

The proposed formalism brings some modeling tools which address some limitations of the resolvent analysis framework. The nonlinear term, assumed to act as an additive Gaussian white
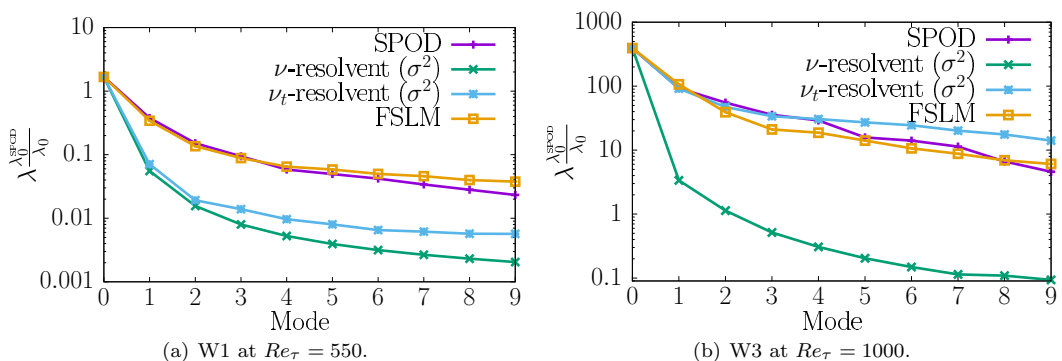

(a) W1 at $Re_\tau = 550$.

(b) W3 at $Re_\tau = 1000$.

FIG. 8. Comparison of the eigenvalues. SPOD eigenvalues λ^{SPOD}, ν-resolvent amplification energy gain $(\sigma^{\nu-\text{resolvent}})^2$ and FSLM spectrum λ^{FSLM} (eigenvalues of $\mathbf{S}^{(n)}$ once converged). The spectra have been normalized by the first SPOD eigenvalue.

noise in resolvent analysis, is constrained in SLM to be issued from a transport mechanism. This can be interpreted in the resolvent framework as playing the role of coloring the additive forcing term. Actually, it is more than this, since it takes explicitly into account inhomogeneity and anisotropy of the turbulent fluctuations. Besides, as explored for instance in Gupta *et al.* [38], there is often—on the basis for instance of the fluctuation dissipation theorem—the requirement to model a random term which brings energy to the system and a diffusion term which dissipates it. The stochastic framework under location uncertainty provides by construction an energy balance between these two mechanisms. For all these reasons, despite its more complex structure, stochastic modeling under location uncertainty may be relevant in flow configurations where resolvent analysis requires finer modeling.

In channel flows, ν-resolvent is accurate only close to the wall for elongated structures (see the Supplemental Material [57] for an overview of the metric $\theta_{\alpha, \beta\gamma}$). Adding eddy viscosity becomes necessary at higher wall-normal locations. In general flow configurations, we do not have systematically a model of eddy viscosity. In such a case a Reynolds-averaged Navier-Stokes (RANS) calculation, which requires a closure as well, allows us to obtain eddy diffusion, as performed for instance in Pickering *et al.* [70]. In the proposed formalism, the stochastic diffusion is deduced from some knowledge of the small-scale statistics, expressed conveniently in terms of velocity fluctuations.

In the present paper, we add the contribution of time-coherent nonlinear interactions. In flows where the main effect lies in small-scale turbulence, the forcing term may be unnecessary. Dedicated studies should be performed to answer this question. However, the nonlinear forcing term appears to be important when nonlinearities arise from interactions between time-coherent structures, such as in wall-bounded flows.

SLM and FSLM are characterized by a modeling degree of freedom through the choice of the parameters ($\bar{\boldsymbol{u}}, \sigma, \mathbf{a}, \tau_s$). We note in particular the role of τ_s, which may be sensitive since it controls the amplitude of the stochastic diffusion. These parameters can be determined based on data or some physical scalings. The proposed strategy in Sec. III D is not universal but aims at minimizing the data requirement. Another possible strategy, which is currently being pursued by our group, is to obtain these parameters without data but only based on a RANS calculation. This can provide the mean flow and also the decorrelation time through the typical time of turbulence dissipation. The tensor σ can be expanded onto resolvent suboptimal modes, as in the present study.

VI. CONCLUSION

In this paper we have proposed a stochastic modeling strategy of coherent structures in turbulent channel flows. By adding a stochastic nonlinear forcing term, we obtain a refinement of the model proposed in Tissot *et al.* [41]. This forced model aims at improving consistency with the physical processes involved in these flows while maintaining the mathematical assumptions of the stochastic formulation. We used this model to explore the prediction abilities in the buffer and logarithmic layers in channels with friction Reynolds number equal to 180, 550, and 1000.

A central ingredient is the incorporation of a nonlinear forcing representing coherent wave-wave interactions, which are essential in the self-sustaining processes of wall-bounded turbulence to generate streamwise vortices for large-scale structures in the logarithmic layer. In the model predictions, such forcing is central in the buffer layer, consistently with the Hamilton-Kim-Waleffe scenario [5]. Moreover, we have shown that it is also central for large-scale structures in the logarithmic layer, which is in line with a large body of evidence in the literature supporting that self-sustaining processes are in action in the logarithmic layer. In addition, the model predicts a significant effect of incoherent turbulence on large log-layer structures, showing that it is crucial to model this effect in order to obtain good predictions. The model that we propose takes into account stochastic transport by this incoherent velocity field leading to an improvement compared to the state-of-the-art ν_t-resolvent analysis. The present model requires a knowledge of the statistics of the turbulent field, and there are some possible open directions concerning its specification.

The modeling ingredients act on several physical mechanisms. First, the stochastic diffusion induced by incoherent velocity field, unlike an eddy viscosity, has the shape of a full tensor with in particular $\langle u'v' \rangle$ off-diagonal components, which are defined consistently with the RMS profiles. A mean drift velocity takes into account the turbophoresis effect (effective transport from high to low turbulence regions), which is active in the buffer layer. A stochastic term representing the lift-up induced by the random incoherent velocity field is explicitly taken into account.

In addition, we have brought technical improvements by ensuring the decorrelation of the incoherent component with the solution through an iterative procedure, and we have proposed an efficient computation of FSLM by reformulating it as a singular value decomposition problem. With these effects taken into account in the model, we obtained an agreement between model predictions and turbulent fluctuations at various wall-normal positions.

In summary, the proposed model incorporates features of resolvent analysis, via the forcing resulting from nonlinear wave-wave interactions, to the stochastic formalism introduced in our previous work [41], combining hence the benefits of the two approaches. The stochastic framework can be seen as a refined model of incoherent turbulence on large-scale structures, which not only includes the standard additional diffusion present in eddy-viscosity models [70,71] but also involves all aspects of stochastic transport at the lengthscale of interest. The study shows that FSLM seems to carry advantageous features for reduced-order modeling of coherent structures in turbulent flows.

ACKNOWLEDGMENTS

[1] S. J. Kline, W. C. Reynolds, F. A. Schraub, and P. W. Runstadler, The structure of turbulent boundary layers, J. Fluid Mech. **30**, 741 (1967).

[2] C. R. Smith and S. P. Metzler, The characteristics of low-speed streaks in the near-wall region of a turbulent boundary layer, J. Fluid Mech. **129**, 27 (1983).

[3] J. Jiménez and P. Moin, The minimal flow unit in near-wall turbulence, J. Fluid Mech. **225**, 213 (1991).

[4] R. L. Panton, Overview of the self-sustaining mechanisms of wall turbulence, Prog. Aerosp. Sci. **37**, 341 (2001).

[5] J. M. Hamilton, J. Kim, and F. Waleffe, Regeneration mechanisms of near-wall turbulence structures, J. Fluid Mech. **287**, 317 (1995).

[6] T. Ellingsen and E. Palm, Stability of linear flow, Phys. Fluids **18**, 487 (1975).

[7] L. Brandt, The lift-up effect: The linear mechanism behind transition and turbulence in shear flows, Eur. J. Mech. B Fluids **47**, 80 (2014).

[8] O. Flores and J. Jiménez, Hierarchy of minimal flow units in the logarithmic layer, Phys. Fluids **22**, 071704 (2010).

[9] A. J. Smits, B. J. McKeon, and I. Marusic, High–Reynolds number wall turbulence, Annu. Rev. Fluid Mech. **43**, 353 (2011).

[10] S. B. Pope, *Turbulent Flows* (Cambridge University Press, Cambridge, UK, 2000).

[11] Y. Hwang and C. Cossu, Self-Sustained Process at Large Scales in Turbulent Channel Flow, Phys. Rev. Lett. **105**, 044505 (2010).

[12] C. Cossu and Y. Hwang, Self-sustaining processes at all scales in wall-bounded turbulent shear flows, Philos. Trans. Roy. Soc. A: Math. Phys. Eng. Sci. **375**, 20160088 (2017).

[13] A. Lozano-Durán, H. J. Bae, and M. P. Encinar, Causality of energy-containing eddies in wall turbulence, J. Fluid Mech. **882**, A2 (2020).

[14] H. J. Bae, A. Lozano-Durán, and B. J. McKeon, Nonlinear mechanism of the self-sustaining process in the buffer and logarithmic layer of wall-bounded flows, J. Fluid Mech. **914**, A3 (2021).

[15] D. Barkley, Linear analysis of the cylinder wake mean flow, Europhys. Lett. **75**, 750 (2006).

[16] P. J. Schmid and D. S. Henningson, *Stability and Transition in Shear Flows*, Vol. 142 (Springer-Verlag, Berlin, 2001).

[17] L. N. Trefethen and M. Embree, *Spectra and Pseudospectra: The Behavior of Nonnormal Matrices and Operators* (Princeton University Press, Princeton, NJ, 2005).

[18] M. R. Jovanović and B. Bamieh, Componentwise energy amplification in channel flows, J. Fluid Mech. **534**, 145 (2005).

[19] B. J. McKeon and A. S. Sharma, A critical-layer framework for turbulent pipe flow, J. Fluid Mech. **658**, 336 (2010).

[20] F. Gómez, A. S. Sharma, and H. M. Blackburn, Estimation of unsteady aerodynamic forces using pointwise velocity data, J. Fluid Mech. **804**, R4 (2016).

[21] S. Symon, D. Sipp, and B. J. McKeon, A tale of two airfoils: Resolvent-based modelling of an oscillator versus an amplifier from an experimental mean, J. Fluid Mech. **881**, 51 (2019).

[22] E. Martini, A. V. G. Cavalieri, P. Jordan, A. Towne, and L. Lesshafft, Resolvent-based optimal estimation of transitional and turbulent flows, J. Fluid Mech. **900**, A2 (2020).

[23] A. Towne, A. Lozano-Durán, and X. Yang, Resolvent-based estimation of space–time flow statistics, J. Fluid Mech. **883**, A17 (2020).

[24] F. R. Amaral, A. V. G. Cavalieri, E. Martini, P. Jordan, and A. Towne, Resolvent-based estimation of turbulent channel flow using wall measurements, J. Fluid Mech. **927**, A17 (2021).

[25] L. Franceschini, D. Sipp, and O. Marquet, Mean- and unsteady-flow reconstruction with one or two time-resolved measurements, arXiv:2102.03839.

[26] C. Leclercq, F. Demourant, C. Poussot-Vassal, and D. Sipp, Linear iterative method for closed-loop control of quasiperiodic flows, J. Fluid Mech. **868**, 26 (2019).

[27] L. I. Abreu, A. V. G. Cavalieri, P. Schlatter, R. Vinuesa, and D. S. Henningson, Resolvent modelling of near-wall coherent structures in turbulent channel flow, Int. J. Heat Fluid Flow **85**, 108662 (2020).

[28] S. Beneddine, D. Sipp, A. Arnault, J. Dandois, and L. Lesshafft, Conditions for validity of mean flow stability analysis, J. Fluid Mech. **798**, 485 (2016).

[29] W. C. Reynolds and A. K. M. F. Hussain, The mechanics of an organized wave in turbulent shear flow. Part 3. Theoretical models and comparisons with experiments, J. Fluid Mech. **54**, 263 (1972).

[30] R. D. Cess, A survey of the literature on heat transfer in turbulent tubeflow, Research Report No. 8-0529-R24 (1958).

[31] Y. Hwang and C. Cossu, Linear non-normal energy amplification of harmonic and stochastic forcing in the turbulent channel flow, J. Fluid Mech. **664**, 51 (2010).

[32] P. Morra, O. Semeraro, D. S. Henningson, and C. Cossu, On the relevance of Reynolds stresses in resolvent analyses of turbulent wall-bounded flows, J. Fluid Mech. **867**, 969 (2019).

[33] S. Symon, S. J. Illingworth, and I. Marusic, Large-scale structures predicted by linear models of wall-bounded turbulence, J. Phys.: Conf. Ser. **1522**, 012006 (2020).

[34] P. Morra, P. A. S. Nogueira, A. V. G. Cavalieri, and D. S. Henningson, The colour of forcing statistics in resolvent analyses of turbulent channel flows, J. Fluid Mech. **907**, A24 (2021).

[35] S. Symon, S. J. Illingworth, and I. Marusic, Energy transfer in turbulent channel flows and implications for resolvent modelling, J. Fluid Mech. **911**, A3 (2021).

[36] S. Symon, A. Madhusudanan, S. J. Illingworth, and I. Marusic, On the use of eddy viscosity in resolvent analysis of turbulent channel flow, arXiv:2205.11216.

[37] P. A. S. Nogueira, P. Morra, E. Martini, A. V. G. Cavalieri, and D. S. Henningson, Forcing statistics in resolvent analysis: application in minimal turbulent Couette flow, J. Fluid Mech. **908**, A32 (2021).

[38] V. Gupta, A. Madhusudanan, M. Wan, S. J. Illingworth, and M. P. Juniper, Linear-model-based estimation in wall turbulence: Improved stochastic forcing and eddy viscosity terms, J. Fluid Mech. **925**, A18 (2021).

[39] A. Zare, M. R. Jovanović, and T. T. Georgiou, Colour of turbulence, J. Fluid Mech. **812**, 636 (2017).

[40] A. Zare, T. T. Georgiou, and M. R. Jovanović, Stochastic dynamical modeling of turbulent flows, Annu. Rev. Control Robot. Auton. Syst. **3**, 195 (2020).

[41] G. Tissot, A. V. G. Cavalieri, and E. Mémin, Stochastic linear modes in a turbulent channel flow, J. Fluid Mech. **912**, A51 (2021).

[42] E. Mémin, Fluid flow dynamics under location uncertainty, Geophys. Astrophys. Fluid Dyn. **108**, 119 (2014).

[43] P. Chandramouli, D. Heitz, S. Laizet, and E. Mémin, Coarse large-eddy simulations in a transitional wake flow with flow models under location uncertainty, Comput. Fluids **168**, 170 (2018).

[44] V. Resseguier, E. Mémin, and B. Chapron, Geophysical flows under location uncertainty, Part I: Random transport and general models, Geophys. Astrophys. Fluid Dyn. **111**, 149 (2017).

[45] V. Resseguier, E. Mémin, and B. Chapron, Geophysical flows under location uncertainty, Part II Quasi-geostrophy and efficient ensemble spreading, Geophys. Astrophys. Fluid Dyn. **111**, 177 (2017).

[46] V. Resseguier, E. Mémin, and B. Chapron, Geophysical flows under location uncertainty, Part III: SQG and frontal dynamics under strong turbulence conditions, Geophys. Astrophys. Fluid Dyn. **111**, 209 (2017).

[47] B. Chapron, P. Dérian, E. Mémin, and V. Resseguier, Large scale flows under location uncertainty: a consistent stochastic framework, Q. J. R. Meteorol. Soc. **144**, 251 (2018).

[48] W. Bauer, P. Chandramouli, B. Chapron, L. Li, and E. Mémin, Deciphering the role of small-scale inhomogeneity on geophysical flow structuration: A stochastic approach, J. Phys. Oceanogr. **50**, 983 (2020).

[49] W. Bauer, P. Chandramouli, L. Li, and E. Mémin, Stochastic representation of mesoscale eddy effects in coarse-resolution barotropic models, Ocean Modell. **151**, 101646 (2020).

[50] B. Pinier, E. Mémin, S. Laizet, and R. Lewandowski, A stochastic flow approach to model the mean velocity profile of wall-bounded flows, Phys. Rev. E **99**, 063101 (2019).

[51] Y. Yang and E. Mémin, High-resolution data assimilation through stochastic subgrid tensor and parameter estimation from 4DEnVar, Tellus A **69**, 1308772 (2017).

[52] Y. Yang and E. Mémin, Estimation of physical parameters under location uncertainty using an Ensemble^2-Expectation-Maximization algorithm, Q. J. R. Meteorol. Soc. **145**, 418 (2019).

[53] P. Chandramouli, E. Mémin, and D. Heitz, 4D large scale variational data assimilation of a turbulent flow with a dynamics error model, J. Comput. Phys. **412**, 109446 (2020).

[54] V. Resseguier, E. Mémin, D. Heitz, and B. Chapron, Stochastic modelling and diffusion modes for proper orthogonal decomposition models and small-scale flow analysis, J. Fluid Mech. **826**, 888 (2017).

[55] V. Resseguier, A. M. Picard, E. Mémin, and B. Chapron, Quantifying truncation-related uncertainties in unsteady fluid dynamics reduced order models, SIAM/ASA J. Uncert. Quantif. **9**, 1152 (2021).

[56] M. Reeks, The transport of discrete particles in inhomogeneous turbulence, J. Aerosol Sci. **14**, 729 (1983).

[57] See Supplemental Material at http://link.aps.org/supplemental/10.1103/PhysRevFluids.8.033904 for complementary results and numerical details.

[58] A. Towne, O. T. Schmidt, and T. Colonius, Spectral proper orthogonal decomposition and its relationship to dynamic mode decomposition and resolvent analysis, J. Fluid Mech. **847**, 821 (2018).

[59] E. Yim, P. Meliga, and F. Gallaire, Self-consistent triple decomposition of the turbulent flow over a backward-facing step under finite amplitude harmonic forcing, Proc. R. Soc. A. **475**, 20190018 (2019).

[60] P. E. Plotter, *Stochastic Integration and Differential Equation*, *Stochastic Modeling and Applied Probability*, Vol. 21 (Springer-Verlag, Berlin, 2005).

[61] R. Moarref, A. S. Sharma, J. A. Tropp, and B. J. McKeon, Model-based scaling of the streamwise energy density in high-Reynolds-number turbulent channels, J. Fluid Mech. **734**, 275 (2013).

[62] J. H. M. Ribeiro, C.-A. Yeh, and K. Taira, Randomized resolvent analysis, Phys. Rev. Fluids **5**, 033902 (2020).

[63] E. Martini, D. Rodríguez, A. Towne, and A. V. G. Cavalieri, Efficient computation of global resolvent modes, J. Fluid Mech. **919**, A3 (2021).

[64] J. Jiménez, Near-wall turbulence, Phys. Fluids **25**, 101302 (2013).

[65] S. Kadri Harouna and E. Mémin, Stochastic representation of the Reynolds transport theorem: revisiting large-scale modeling, Comput. Fluids **156**, 456 (2017).

[66] J. F. Gibson, F. Reetz, S. Azimi, A. Ferraro, T. Kreilos, H. Schrobsdorff, M. Farano, A. F. Yesil, S. S. Schütz, M. Culpo, and T. M. Schneider, 2019 Channelflow 2.0. Available at: https://www.channelflow.ch/.

[67] A. V. G. Cavalieri, P. Jordan, and L. Lesshafft, Wave-packet models for jet dynamics and sound radiation, Appl. Mech. Rev. **71**, 020802 (2019).

[68] A. V. G. Cavalieri, D. Rodríguez, P. Jordan, T. Colonius, and Y. Gervais, Wavepackets in the velocity field of turbulent jets, J. Fluid Mech. **730**, 559 (2013).

[69] J. C. Del Álamo and J. Jiménez, Linear energy amplification in turbulent channels, J. Fluid Mech. **559**, 205 (2006).

[70] E. Pickering, G. Rigas, O. T. Schmidt, D. Sipp, and T. Colonius, Optimal eddy viscosity for resolvent-based models of coherent structures in turbulent jets, J. Fluid Mech. **917**, A29 (2021).

[71] C. Cossu, G. Pujals, and S. Depardon, Optimal transient growth and very large–scale structures in turbulent boundary layers, J. Fluid Mech. **619**, 79 (2009).